RSC Advances

ROYAL SOCIETY OF CHEMISTRY

www.rsc.org/advances

Contrastive band gap engineering of strained graphyne nanoribbon with armchair and zigzag edges

Xin Cong, Yiming Liao, Qiji Peng, Yidan Yang, Chuan Cheng, Wenqing Zhang, Peilin Fang, Chi Chen, Ling Miao* and Jianjun Jiang

School of Optical and electronical Information, Huazhong University of Science and Technology, Wuhan, HUBEI 430074, People's Republic of China.

*Email: miaoling@mail.hust.edu.cn

Abstract

The band gap engineering of nano-structure is the key point in application of nano electronic device. By using first-principles calculations, the band structures of graphyne nanoribbons with armchair (a-GNRs) and zigzag (z-GNRs) edges under various strains are investigated. A controllable band gap of strained narrow a-GNR (1.36~2.85 eV) could be modulated almost linearly under an increasing strain in range of －5% ~ 16%. In contrast, the band gap of strained narrow z-GNR (2.68 ~ 2.91 eV) is relatively insensitive to －16% ~ 16% strain. This contrastive band gap engineering of narrow GNRs is attributed to different structure deformation of the specific graphyne structure including two kinds of carbon atoms different from graphene. For wider strained GNRs, the band gap depending on its width and edge morphology generally decreases as tensile strain increases, similar to 2D graphyne sheet. The charge density distributions of key states around Fermi level are presented

to investigate the reason of band gap variation.

Introduction

Graphyne, a fantastic 2D carbon nanostructure like graphene, attracts tremendous attentions due to the super properties, such as large carrier mobility[1], relatively low in-plane Young's modulus (162 N/m)[2], anisotropic optical property and Possion ratio[3]. Furthermore, different graphyne structures possess diverse electrical characters, like good electrical conduction[4] and native band gap[5-7]. It is important since the band gap engineering is the key point in application of nano electronic device. Many strategies to tune band gap of nano-structure have been studied intensively. For examples, a finite value band gap of graphene is obtained by tailoring the 2D graphene sheet into nanoribbons with different widths[8-11] and edges[12-14], the band gap of silicon nanowire is modified by saturating the silicon surface[15] and uniaxial strain[16], and the band gap of phosphorus is modulated by stacking order[17] and tailoring into nanoribbon along three orientations with various strains[18, 19].

Meanwhile, the similar approaches have been also applied to modulate the band gap of graphyne, including tailoring graphyne sheet into graphyne nanoribbon (GNR)[20], loading strain, stacking multilayer graphyne[21], and doping with boron or nitrogen atoms[22]. Especially, the band gap of z-GNR shows a unique “step effect” as the width increases[20]. The band gap of 2D graphyne sheet is influenced by homogeneous biaxial strain[3]. Similarly, graphdiyne is cut to obtain graphdiyne nanoribbon whose band gap decreases monotonically as the width increases[20, 23]. The

tunable band gap of graphdiyne monotonously increases with uniform increasing strain[24]. A plenty of previous works investigating the strain influencing on mechanical and electronical properties of graphyne, show tremendous potential applications for novel strain-tunable nanoelectronic and optoelectronic devices[25-28]. However, the response of band gap of GNR to the uniaxial tensile and compressive strains has little been reported. To insight it, a systematic investigation of strain effect on band gap of GNR is desperately needed.

In this paper, we investigate the critical compressive strain of GNRs and the response of band gap of graphyne nanoribbons to the homogeneous uniaxial strain, by first principle calculations. To reveal the effect of edge morphology and carbon hybrid orbitals, GNRs with narrow width and wide width are investigated separately. The band structures, charge density distributions and projected density of states (PDOS) are calculated to analyze the law of band gap variation.

Computational Methods

All calculations are carried out by SIESTA code[29] with the framework of density function theory (DFT)[30, 31]. Local density approximation described by Ceperley-Alder[32] is chosen as the exchange correlation potential, and the Troullier-Martins scheme norm-conserving pseudopotentials[33] is employed to represent the interaction between localized pseudoatomic orbitals and ionic cores. The double-ζ basis plus polarization orbital set is adopted to ensure a good computational convergence. The energy cutoff is 120 Ry. The Brillouin zone sampling is performed

using a Monkhorst-Pack special k points gird[34]. All structures are fully relaxed with the force on each atom less than 0.05 eV/Å. A vacuum layer of 10 Å in the supercell is designed to render the interaction between the GNR layer and its periodic image negligible.

Results and Discussions

The graphyne structure is optimized and the lattice constants of 6.92 Å is in agreement with the previous result[3, 20]. The graphyne sheets are cut along X direction and Y direction to obtain a-GNRs and z-GNRs as shown in Fig. 1, respectively. The nanoribbon edge is passivated with hydrogen atoms like similar works[20]. In our work, a series of a-GNRs (n=1 ~ 5) and z-GNRs (n=1 ~ 4) are investigated with the maximal width about 28.89 Å, here n indicates the number of repeated chains of benzene ring. Each nanoribbon is strained within the range of the critical compressive strain to 16% tensile strain by scaling the lattice constant.

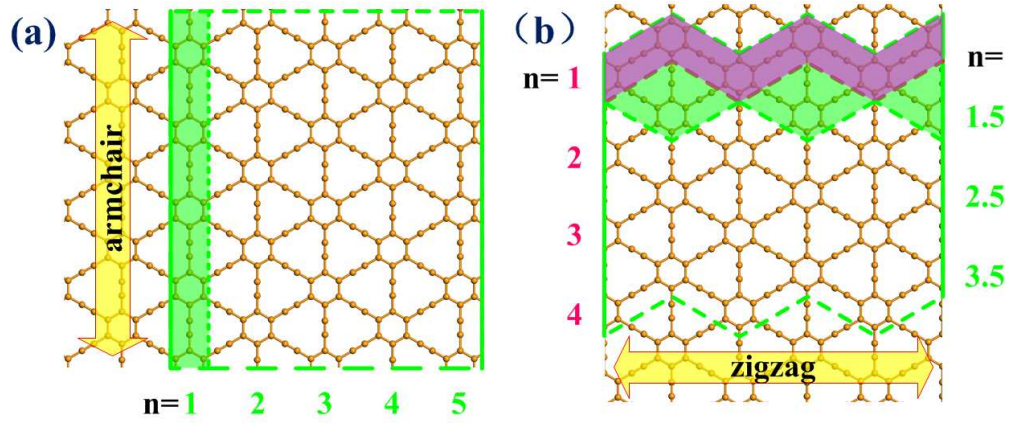

Fig. 1. Schematic representation of graphyne nanoribbons of two edges. (a) a-GNR cut along Y (armchair) direction, and (b) z-GNR cut along X (zigzag) direction.

For very thin films, the large compressive strain will induce out-of-plane

buckling and undulation, and it is much smaller than the critical tensile strain for fracture, such as 2D graphene sheet that the critical compressive strain is several orders of magnitude smaller than the critical tensile strain[35]. So, before the investigating variation of strained GNRs, the critical compressive strain should be identified to ensure stable and realistic structure. The structures of strained GNRs are initial buckling or undulation, by moving atoms out-of-plane artificially (Figure S1, Supporting Information). And the structures with initial plane are also calculated. At a specific compressive strain, difference value of energy with two initializations is changed, from positive to negative (Figure S3, Supporting Information). And this strain is chosen as critical compressive strain. The critical compressive strain of all GNRs ascertained (presented in Table SI). Particularly, z-GNR of n=1 withstands larger compressive strain than 16%, and the critical compressive strain (2%~3%) of other z-GNRs show a zigzag variation as width increase. And the maximal compressive strain of a-GNRs is about 4%.

A-GNRs and z-GNRs with narrow width

We firstly focus on the strained GNRs with narrow width, and take width n=1 for example here. Their band structures around Fermi level and corresponding tendency of band gap variation under strain are given in Fig. 2(a). The band structure detail of zero-strain a-GNR and z-GNR are also shown in Fig. 2(b, d), and their calculated band gaps are in good agreement with tendency of previous result[20]. It could be found that a controllable band gap of strained a-GNR in range of 1.36 ~ 2.85 eV could be

modulated almost linearly under an increasing strain. Contrasting with a-GNR spectacularly, the band gap of strained z-GNR (2.68 ~ 2.91 eV) with narrow widths is little influenced by strain.

The band structure of unstrained a-GNR (in Fig. 2(b)) shows a direct band gap at X point. And from the inserts in Fig. 2(a), we could find that the modulated band gap is due to the fall of the valence band maximum (VBM) energy and the rise of the conduction band minimum (CBM) energy under increasing strain. The charge density distributions (isovalue = 0.008 e/Å^3) at CBM and VBM states of a-GNR shown in Fig. 2(c) visualize the main contribution from the bonds in a-GNR structure. Similarly, z-GNR has a direct band gap at Γ point. Its band gap is little influenced by strain due to VBM and CBM retain at Γ point with little variation under various strain. And the corresponding charge density distributions of these key states are also visualized in Fig. 2(e), respectively.

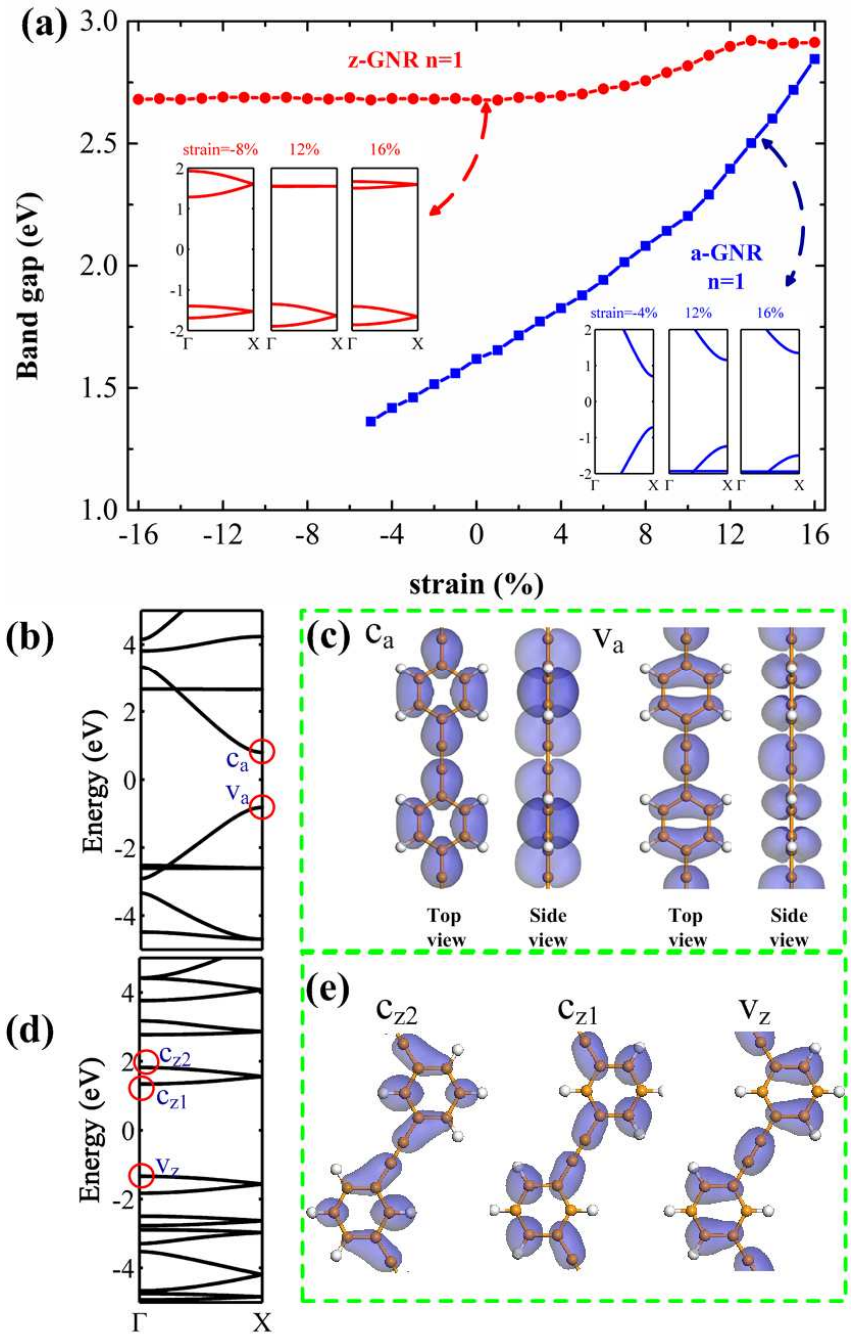

Fig. 2. (a) Band gap variation of strained a-GNR and z-GNR with widths n=1, inset is a plot of strained band structure of a-GNR and z-GNR. (b) Band structures and (c) charge density distribution (isovalue=0.008 e/Å^3) for different states of a-GNR (n=1) without strain. (d) Bands structure and (e) charge density distribution for different states of z-GNR (n=1) without strain.

Subsequently, the variation of bonds lengths and bond angles in strained GNR

structures are listed in Fig. 3. For a-GNR, the lengths of C1−C2 (1.37 ~ 1.45 Å) and C3−C4 (1.37 ~ 1.74 Å) bonds increase remarkably along with strain growing. The interaction of atoms connected with these stretched bonds will have a large change, and lead to the rise of $\mathbf{c}_a$ state energy and the fall of $\mathbf{v}_a$ state energy, showing as the enlarging of band gap.

On the contrary, the length of bonds in z-GNR occur little variation, especially under small strains. It is interesting that strain primarily influence the bond angle of C3−C4−C5, due to the unparallel strain direction with acetylenic bond in z-GNR structure. The primary change occurring in bond angle instead of length results in little variation of CBM and VBM states, which determines an almost invariable band gap around 2.7 eV as shown in Fig. 2(b). Under lager strain, the acetylenic bond will get close to the strain direction, and the lengths of bond, instead of the bond angle, show a perceptible variation. Meanwhile the band gap of z-GNR has a gradual raise under +8% ~ +12% strains. And the strain, primarily influencing bond length, shift CBM from $\mathbf{c}_{z1}$ state to $\mathbf{c}_{z2}$ state, resulting in a wider band gap.

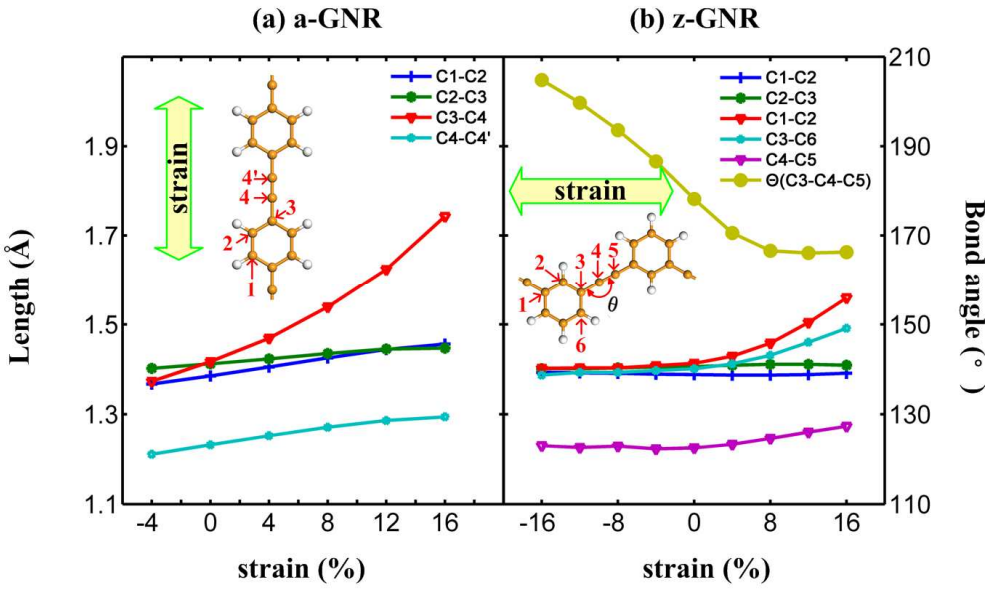

Fig. 3. Structure variations of strained (a) a-GNR and (b) z-GNR of n=1 under strains.

It is obvious that the band gaps of a-GNR and of z-GNR have different response to various strains. Strain primarily influences bond lengths of a-GNR, which results in almost linear increase of band gap. On the contrary, due to bond angle variation leading to little variation of bond lengths, the band gap of z-GNR has insensitive response to strain.

A-GNRs with wide widths

So far, the calculations come to the conclusion of the band gap variation with narrow width under strain. Then the influences of strain on band gap of a-GNRs as width widen, are investigated. The band gaps of a-GNRs decrease as the width increases with same strain [see Fig. 4(a)] which is good agreement with previous work[20]. It is obvious that for wider strained a-GNRs, the band gap depending on its width and edge morphology generally decreases as tensile or compressive strain

increases, similar to 2D graphyne sheet[36].

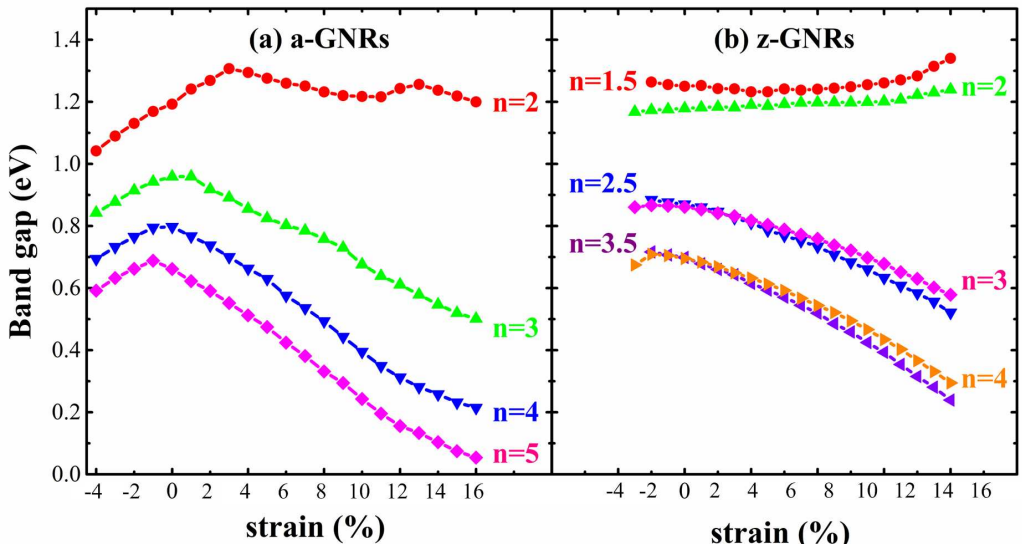

Fig. 4. Band gap variation of a-GNRs and z-GNRs with different widths under strain.

In Fig. 5(a), the band structures which are almost symmetric about fermi level detailly show the unstrained band gaps. Due to the similar band structures and variation tendencies of band gap under various strain (see Fig. 4(a)), a-GNRs of n=3 are taken as example to reveal the tendency of band gap with various strain, which is different from that of a-GNR (n=1).

Under compressive or tensile strain (−4% ~ +16%), the band gap of a-GNR (n=3) possesses monotonic decreasing within the range from 0.84 to 0.96 eV. With approximate width, the band gap of armchair graphene nanoribbon (0.2 eV ~ 1.2 eV) demonstrates a zigzag behavior under −16% ~ +16% strain[37], while the band gap of armchair phosphorene nanoribbons (0.4 eV ~ 1.0 eV) monotonously increases under −10% ~ +10% strain[18] and the band gap variation of [110] silicon nanowire shows similar to a-GNR (n=3) within the range from 1.3 eV to 1.8 eV under -5% ~ +5% strain[38].

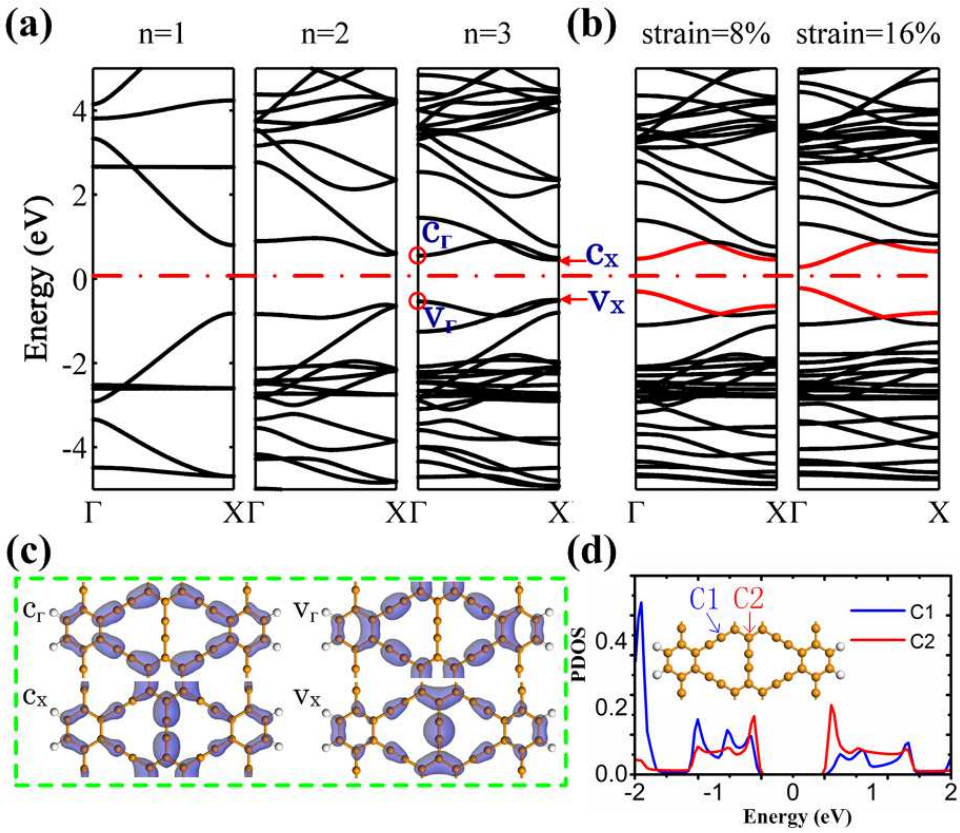

Fig. 5. (a) Band structures of a-GNR with different widths (n=1, 2 and 3). (b) Band structures of a-GNR of n=3 under typical strains (4% and 16%). Here Fermi level (red dashed line) is at zero. (c) Charge density distributions for different states in a-GNR of n=3 with zero strain, (Isovalue=0.008 e/Å^3). (d) 2***p*** orbital PDOS of two different carbon atoms.

The band gap of a-GNRs of n=3 is calculated according $\mathbf{c}_\Gamma$, $\mathbf{v}_\Gamma$, $\mathbf{c}_X$ and $\mathbf{v}_X$ states on a couple bands at Γ and X points under different strains, as shown in Fig. 5(b). Under compression or zero strain, the band gap is determined at $\mathbf{c}_X$ and $\mathbf{v}_X$ states. Their charge distributions presented in Fig. 5(c) primarily locate at edge atoms, which is similar to a-GNR of n=1. Similar charge distributions result in similar incremental variation in band gap. As strain turns tensile, the band gap of a-GNR is determined at $\mathbf{c}_\Gamma$, $\mathbf{v}_\Gamma$, $\mathbf{c}_X$ and $\mathbf{v}_X$ states. And their charge distributions primarily locate at non-edge

atoms, similar to that of pure graphyne[36], resulting a declining variation in band gap. The energies of these CBM and VBM states have different response to strain, leading to a shift of band structure from direct to indirect band gap, under +4% ~ +12% strains.

Especially, the band gap variation tendency under tensile strain is primarily due to the inner atoms situated in the body of a-GNRs. This result verifies the declining tendency of band gap as width widen. Owning to enhancing proportion of non-edge charge distribution, the variation tendency of band gap of GNR with wider width will tend to the same of graphyne[36], because the nanoribbon will return to a 2D structure. Furthermore, these inner atoms are divided into two types, one atom linked by acetylenic bond and another resided within benzene ring. The 2***p*** orbital PDOS of two different carbon atoms in Fig. 5(d) proves that the carbon atom resided within benzene ring influences band gap primarily, good agreement with previous work.[3, 20]

Z-GNRs with wide widths

As width of z-GNR increases, the band gap of unstrained z-GNRs shows a step decrease in Fig. 4(b) and Fig. 6(a), which is in good agreement with previous work[20]. And their band gap shows declining tendency under tensile strain, like a-GNRs.

We take two z-GNRs (n=2.5, 3) as example for following investigations, due to the consistent band gap variation. Under strain (-2% ~ +16%), the band gap of z-GNR (n=2.5) possesses monotonic decreasing within range of 0.52 to 0.88 eV. With approximate width, the band gap of zigzag graphene nanoribbon (0.2 eV ~ 0.3 eV)

monotonously increases under −15% ~ +15% strain[39], while the band gap of zigzag phosphorene nanoribbons (0.7 eV ~ 1.4 eV) increases firstly, then decreases under −10% ~ +10% strain[18] similar to z-GNRs and the band gap of zigzag boron nitride nanoribbon (2.3 eV ~ 4.0 eV) decreases monotonously under 0 ~ 12% strain[40].

To investigate the band gap variation, the band structures of unstrained z-GNRs are presented in Fig. 6(a). The calculated band structures revel that the energy of $\mathbf{v}_x$ state obviously rises, while the other states around Fermi level almost remain the same under different strains. The band structure remains direct gap ($\mathbf{v}_x$ state and $\mathbf{c}_x$ state at X point in Fig. 6(a)) under positive strain.

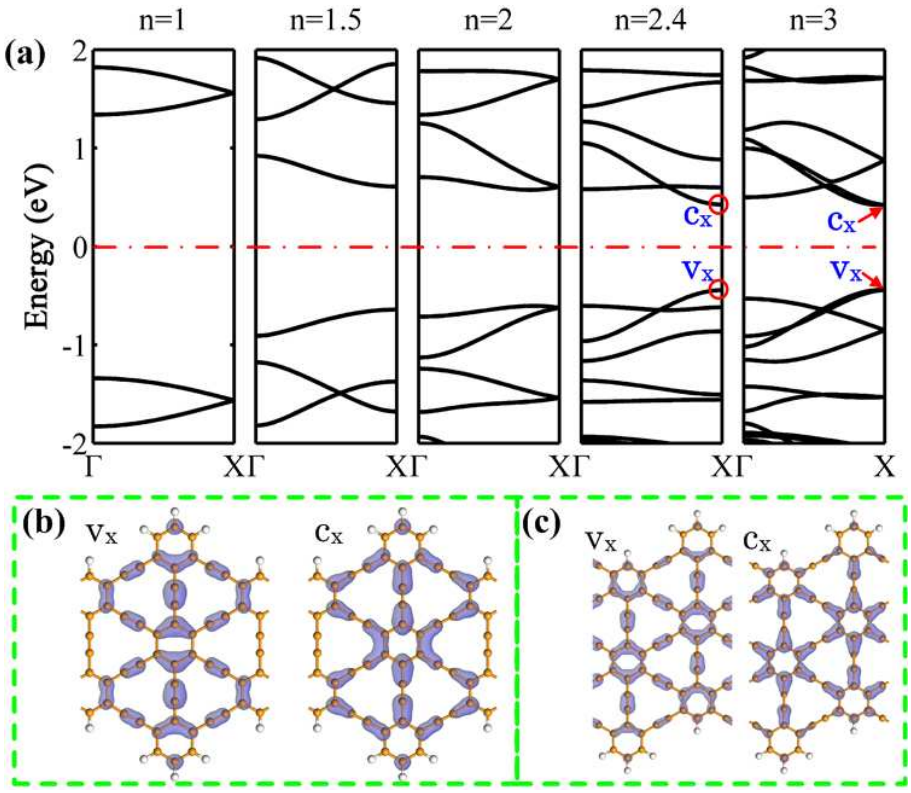

Fig. 6 (a) Band structures of z-GNRs with widths range from n=1 to n=3. Here Fermi level is at zero. Charge density distributions for different states in unstrained z-GNRs of (c) n=2.5 and (d) n=3 (isovalue=0.008 e/Å^3).

The step decrease of band gap of z-GNRs could be explained by comparing Fig. 6(b) with 6(c). The z-GNRs with widths n=2.5 and n=3 have similar charge distributions at $\mathbf{c}_x$, $\mathbf{c}_\Gamma$ and $\mathbf{v}_\Gamma$ states, except for the edge of $\mathbf{v}_x$ state. The similar charge distributions result in similar band gap variation of z-GNRs (n=2.5, 3) under strain. It could be also found that the charge distributions at inner region of z-GNRs are similar to that of a-GNRs in Fig. 5(b). The non-edge charge distributions are primarily contributed by inner benzene ring carbon like a-GNRs case, leading to similar tendency to a-GNRs, in Fig. 4(b). For example, the band gap of z-GNR and a-GNR of n=3 reduce as tensile strain increases. Furthermore, the edge morphology gives rise to different submarginal charge distribution, which will cause slight difference variation of band gap between a-GNRs and z-GNRs.

Conclusions

In summary, a series of band gap of strained a-GNR (n=1 ~ 5) and z-GNR (n=1 ~ 4) are investigated by using first-principle calculation. The z-GNR of n=1 can be taken a wide range of strain (-16% ~ +16%). A controllable band gap of strained a-GNR (n=1) in the range of 1.36~2.85 eV could be modulated almost linearly, due to the lengths of C1-C2 (1.37 ~ 1.45 Å) and C3-C4 (1.37 ~ 1.74 Å) bonds increasing remarkably under an increasing strain. The band gap of strained z-GNR (2.68 ~ 2.92 eV) with width n=1 is slightly influenced by strain owing to the fact that strain primarily influences the bond angle of C3-C4-C5 instead of bonds length. The band gap of a-GNRs experiences a direct-to-indirect gap transition with sufficient strain.

For wide width, the band gap of GNRs depending on its width and edge morphology generally decreases as tensile strain increases. With width of z-GNR increasing, the band gap of strained z-GNRs shows a step decrease. The band gap of GNRs has a wide controllable range from 0.05 to 2.92 eV. Thus, our work provides an efficient method including edge morphology, width and strain for modulating band gap of GNRs which shows great potential application of GNRs in novel strain-tunable nanoelectronic devices.

Acknowledge

This research work was supported by Fundamental Research Funds for the Central Universities (HUST 15A71).

1. J. Chen, J. Xi, D. Wang and Z. Shuai, *The Journal of Physical Chemistry Letters*, 2013, **4**, 1443-1448.
2. Q. Peng, W. Ji and S. De, *Physical Chemistry Chemical Physics*, 2012, **14**, 13385-13391.
3. J. Kang, J. Li, F. Wu, S.-S. Li and J.-B. Xia, *The Journal of Physical Chemistry C*, 2011, **115**, 20466-20470.
4. H. Sevinçli and C. Sevik, *Applied Physics Letters*, 2014, **105**, 223108.
5. R. Baughman, H. Eckhardt and M. Kertesz, *The Journal of chemical*

physics, 1987, **87**, 6687-6699.

6. V. Coluci, S. Braga, S. Legoas, D. Galvao and R. Baughman, *Physical Review B*, 2003, **68**, 035430.
7. N. Narita, S. Nagai, S. Suzuki and K. Nakao, *Physical Review B*, 1998, **58**, 11009.
8. Q. Yan, B. Huang, J. Yu, F. Zheng, J. Zang, J. Wu, B.-L. Gu, F. Liu and W. Duan, *Nano letters*, 2007, **7**, 1469-1473.
9. M. Y. Han, B. Özyilmaz, Y. Zhang and P. Kim, *Physical review letters*, 2007, **98**, 206805.
10. L. Yang, C.-H. Park, Y.-W. Son, M. L. Cohen and S. G. Louie, *Physical Review Letters*, 2007, **99**, 186801.
11. V. Barone, O. Hod and G. E. Scuseria, *Nano letters*, 2006, **6**, 2748-2754.
12. O. Hod, J. E. Peralta and G. E. Scuseria, *Physical Review B*, 2007, **76**, 233401.
13. D.-e. Jiang, B. G. Sumpter and S. Dai, *The Journal of chemical physics*, 2007, **126**, 134701.
14. Y. Lu, R. Wu, L. Shen, M. Yang, Z. Sha, Y. Cai, P. He and Y. Feng, *Applied Physics Letters*, 2009, **94**, 122111.
15. M. Nolan, S. O'Callaghan, G. Fagas, J. C. Greer and T. Frauenheim, *Nano letters*, 2007, **7**, 34-38.
16. K.-H. Hong, J. Kim, S.-H. Lee and J. K. Shin, *Nano letters*, 2008, **8**,

1335-1340.

17. J. Dai and X. C. Zeng, *The Journal of Physical Chemistry Letters*, 2014, **5**, 1289-1293.
18. X. Han, H. Morgan Stewart, S. A. Shevlin, C. R. A. Catlow and Z. X. Guo, *Nano letters*, 2014, **14**, 4607-4614.
19. X. Peng, Q. Wei and A. Copple, *Physical Review B*, 2014, **90**, 085402.
20. L. Pan, L. Zhang, B. Song, S. Du and H.-J. Gao, *Applied Physics Letters*, 2011, **98**, 173102.
21. O. Leenaerts, B. Partoens and F. Peeters, *Applied Physics Letters*, 2013, **103**, 013105.
22. H. Bu, M. Zhao, H. Zhang, X. Wang, Y. Xi and Z. Wang, *The Journal of Physical Chemistry A*, 2012, **116**, 3934-3939.
23. H. Bai, Y. Zhu, W. Qiao and Y. Huang, *RSC Advances*, 2011, **1**, 768-775.
24. Y. Pei, *Physica B: Condensed Matter*, 2012, **407**, 4436-4439.
25. Y. Yang and X. Xu, *Computational Materials Science*, 2012, **61**, 83-88.
26. Y. Zhang, Q. Pei and C. Wang, *Applied Physics Letters*, 2012, **101**, 081909.
27. S. W. Cranford, D. B. Brommer and M. J. Buehler, *Nanoscale*, 2012, **4**, 7797-7809.

28. S. W. Cranford and M. J. Buehler, *Carbon*, 2011, **49**, 4111-4121.

29. J. M. Soler, E. Artacho, J. D. Gale, A. García, J. Junquera, P. Ordejón and D. Sánchez-Portal, *Journal of Physics: Condensed Matter*, 2002, **14**, 2745.

30. I. E. Gas, P. Hohenberg, W. Kohn, S.-C. E. I. Exchange and L. Sham, *Phys. Rev*, 1964, **136**, B864.

31. W. Kohn and L. J. Sham, *Physical Review*, 1965, **140**, A1133.

32. D. M. Ceperley and B. Alder, *Physical Review Letters*, 1980, **45**, 566.

33. N. Troullier and J. L. Martins, *Physical Review B*, 1991, **43**, 1993.

34. H. J. Monkhorst and J. D. Pack, *Physical Review B*, 1976, **13**, 5188.

35. Y. Zhang and F. Liu, *Applied Physics Letters*, 2011, **99**, 241908.

36. Q. Yue, S. Chang, J. Kang, S. Qin and J. Li, *The Journal of Physical Chemistry C*, 2013, **117**, 14804-14811.

37. X. Peng and S. Velasquez, *Applied Physics Letters*, 2011, **98**, 023112.

38. D. Shiri, Y. Kong, A. Buin and M. Anantram, *Applied Physics Letters*, 2008, **93**, 073114.

39. Y. Lu and J. Guo, *Nano Research*, 2010, **3**, 189-199.

40. J. Qi, X. Qian, L. Qi, J. Feng, D. Shi and J. Li, *Nano letters*, 2012, **12**, 1224-1228.